Rotational Diffusion in Iron Ferrofluids

ARTICLE *in* LANGMUIR · SEPTEMBER 2003

Impact Factor: 4.46 · DOI: 10.1021/la0346393

Rotational Diffusion in Iron Ferrofluids

Ben H. Erné,* Karen Butter, Bonny W. M. Kuipers, and Gert Jan Vroege

Van 't Hoff Laboratory for Physical and Colloid Chemistry, Debye Institute, Utrecht University, Padualaan 8, 3584 CH Utrecht, The Netherlands

Received April 15, 2003. In Final Form: July 18, 2003

The dynamic magnetic susceptibility of relatively monodisperse iron ferrofluids was measured from 1 Hz to 100 kHz for different sizes of the iron particles (all with a 7-nm-thick organic surface layer, dispersed in Decalin). In the case of particles with an iron core of 6-nm radius, the orientation of the magnetic dipole moment thermally rotated inside the particles (Néel rotation). In the case of particles with a slightly larger iron core, the orientation of the magnetic dipole moment was blocked inside the particles but could still change by rotational diffusion of the particles themselves (Brownian rotation). With even larger particles (above 7-nm iron core radius), aggregates were formed: the rotational diffusion rate was lower than that of single particles by more than 1 order of magnitude. This sudden appearance of aggregates above a certain size of the iron particles agrees with previous observations in two dimensions, by cryogenic transmission electron microscopy of ultrathin ferrofluid films. Here, it is found that the threshold for aggregation is practically the same in three dimensions. Moreover, the rotational diffusion rate of the aggregates is seen to increase upon dilution, indicating a decrease in aggregate size. This suggests that a dynamic equilibrium exists between the sticking of particles to each other and unsticking, especially when the particles are sufficiently small so that the sticking energy is not more than a few times the thermal energy.

Introduction

Ferrofluids are colloidal dispersions of magnetic nanoparticles with a single magnetic domain.[1−3] They are used in several commercial applications[4,5] and as model systems in fundamental work on dipolar fluids.[6−8] When the magnetic interaction between particles is sufficiently strong, they form aggregates. In a previous study,[9−11] anisotropic aggregation was observed as a function of the particle size using a series of iron ferrofluids. The aggregates were imaged using cryogenic electron microscopy (cryo-TEM). Here, the same iron ferrofluids are investigated by measuring the dynamic magnetic susceptibility, giving new information about the rotational diffusion of single particles and aggregates.

The series of ferrofluids consists of relatively monodisperse metallic iron particles (10−15% polydispersity) with a 7-nm-thick organic surface layer, dispersed in the solvent Decalin. The low polydispersity is important for the interpretation because the magnetic interaction energy between two monodomain particles is extremely sensitive to the particle size (see Theory section). When ferrofluid samples were prepared for cryo-TEM in the previous study,[9−11] they were cooled so rapidly that the solvent vitrified and the magnetic particle positions remained unchanged. Films of dispersions could, therefore, be studied in situ. Figure 1 summarizes those results (except for ferrofluid A, which had even smaller particles than ferrofluid B and was only weakly magnetic). No aggregates are observed for the ferrofluids with the smallest particles

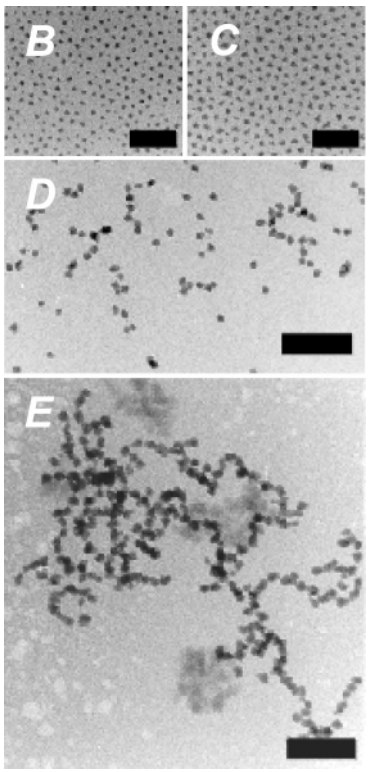

Figure 1. Cryo-TEM pictures of ferrofluids consisting of metallic iron particles with a 7-nm-thick organic surface layer dispersed in Decalin.[9−11] The radius of the iron core gradually increases from ferrofluid B (6 nm) to ferrofluid E (8 nm). The scale bars are 100 nm.

* To whom correspondence should be addressed. E-mail: b.erne@chem.uu.nl.

(1) Rosensweig, R. E. *Sci. Am.* **1982**, *247* (Oct), 124.
(2) Rosensweig, R. E. *Ferrohydrodynamics*; Cambridge University Press: Cambridge, 1985.
(3) Charles, S. W. In *Studies of Magnetic Properties of Fine Particles and their Relevance to Materials Science*; Dormann, J. L., Fionari, D., Eds.; North-Holland: Amsterdam, 1992; p 267.
(4) *Magnetic Fluids and Applications Handbook*; Berkovski, B., Bashtovoy, V., Eds.; Begel House, Inc.: New York, 1996.
(5) Raj, K.; Moskowitz, R. *J. Magn. Magn. Mater.* **1990**, *85*, 233.
(6) Cabuil, V. *Curr. Opin. Colloid Interface Sci.* **2000**, *5*, 44.
(7) Teixeira, P. I. C.; Tavares, J. M.; Telo da Gama, M. M. *J. Phys.: Condens. Matter* **2000**, *12*, R411.
(8) Charles, S. W. *Chem. Eng. Commun.* **1988**, *67*, 145.
(9) Butter, K.; Bomans, P. H.; Frederik, P. M.; Vroege, G. J.; Philipse, A. P. *Nature Mater.* **2003**, *2*, 88.
(10) Butter, K.; Philipse, A. P.; Vroege, G. J. *J. Magn. Magn. Mater.* **2002**, *252*, 1.
(11) Butter, K.; Bomans, P. H.; Frederik, P. M.; Vroege, G. J.; Philipse, A. P. *J. Phys.: Condens. Matter* **2003**, *15*, S1451.

10.1021/la0346393 CCC: $25.00
Published on Web 09/03/2003

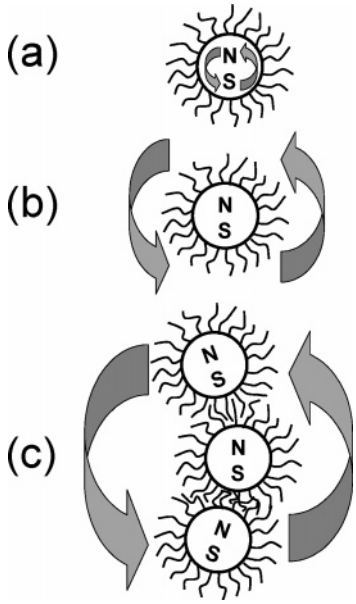

Figure 2. Schematic illustration of the mechanisms that lead to a change in the orientation of the magnetic dipole moments of ferrofluid particles: (a) Néel rotation of the magnetic moment inside a particle, (b) Brownian rotation of a single particle, and (c) Brownian rotation of an aggregate. The magnetic poles are indicated by "N" and "S".

(B and C). The slightly larger D particles show chainlike aggregates of a few particles, and the ferrofluid with the largest particles (E) shows larger aggregates with branched chains.

Compared to scattering techniques, which yield results in reciprocal space and whose interpretation is model-dependent, cryo-TEM has the advantage of giving a direct image of the ferrofluid structure, without the strong drying effects obtained with conventional TEM. Nevertheless, aggregates seen by cryo-TEM are not the same as those in bulk ferrofluid. During sample preparation, before vitrification, a thin film of ferrofluid is made that is not much thicker than the magnetic particles themselves. Any aggregates seen by cryo-TEM are, therefore, two-dimensional, whereas aggregates in bulk ferrofluid can be branched in three dimensions. The magnetic susceptibility spectra in the present paper are complementary to the cryo-TEM results because they probe aggregates as they occur in bulk ferrofluid. Moreover, the magnetic susceptibility measurements are easily performed as a function of the concentration, in contrast to cryo-TEM, for which the two-dimensional concentration is difficult to control.

The frequency dependence of the magnetic susceptibility tells how fast the magnetic dipole moments in a ferrofluid reach a new steady-state average orientation when a magnetic field is applied.[12] In the measurements of the present work, the applied magnetic field is so weak that reorientation occurs by thermal motion. One possible mechanism is that the magnetic dipole moment rapidly rotates inside the particles (Néel rotation, Figure 2a). Otherwise, if the orientation of the magnetic dipole is locked within the particles, entire particles or aggregates must rotate (respectively parts b and c of Figure 2). The Brownian rotation rate of single spheres is a well-known function of the particle radius and the solvent viscosity (see Theory), whereas the Brownian rotation of an aggregate is much slower and should depend on the size, shape, and flexibility of the aggregate. Determining the frequency up to which the magnetization of a ferrofluid can be modulated using an alternating magnetic field is a way to characterize the magnetic particles or aggregates.

The following section recalls general theory about the magnetization of ferrofluids in a constant or alternating external magnetic field. The Experimental Section refers to the synthesis and characterization of the ferrofluids and describes the dynamic magnetic susceptibility setup. This is followed by Results and a separate Discussion.

Theory

The magnetic properties of ferrofluids are introduced, with emphasis on the dynamic magnetic susceptibility. A more complete presentation of this technique was authored by Fannin,[12] and general reviews of the properties of magnetic fluids can be found in refs 1−3.

Because each magnetic particle in the ferrofluid has a single magnetic domain, the magnetic dipole moment μ of a particle is given by its volume times the saturation magnetization per unit volume, m_S. When the assumption is made that the particles are spherical with a magnetic radius a_M, μ is given by

$$\mu = (4/3)\pi {a_M}^3 m_S \tag{1}$$

In other ferrofluids, the magnetic radius a_M was observed to be somewhat smaller than the physical radius a_{core} of the sphere of magnetic material, an effect that was ascribed to the pinning of spins near the surface as a result of interaction with surfactant molecules.[3] The interaction energy U between two particles depends on the magnitude and orientations of the dipole moments $\vec{\mu}_1$ and $\vec{\mu}_2$ and the separation vector $\vec{r}$ (with amplitude r) between the centers of the particles:

$$U = \frac{\mu_0}{4\pi}\left[\frac{\vec{\mu}_1 \cdot \vec{\mu}_2}{r^3} - \frac{3(\vec{\mu}_1 \cdot \vec{r})(\vec{\mu}_2 \cdot \vec{r})}{r^5}\right] \tag{2}$$

where μ_0 is the permeability of vacuum. The attraction is maximal in the head-to-tail orientation, and with the assumption that all the particles are alike, it is given by

$$U_{max} = \frac{-\mu_0}{2\pi}\left[\frac{\mu^2}{(2a)^3}\right] \tag{3}$$

where a is the physical radius of the particles, including the surfactant layer, and $2a$ is the closest distance at which the particles can approach each other. Note that, because of eq 1, this scales with ${a_M}^6/a^3$. Aggregation is expected when $-U_{max}$ is above $\approx 2k_BT$, where k_BT is the thermal energy.[13−16] In Figure 3, eq 3 was used to calculate $-U_{max}/k_BT$, using the saturation magnetization of our carbon-containing iron material (see Experimental Section) and assuming a difference of 1.5 nm between a_{core} and a_M and an organic surface layer of 7.0 nm ($a - a_{core}$).

Magnetization in a Constant Magnetic Field. In zero external magnetic field, the orientations of the magnetic dipoles are isotropically distributed in all directions, resulting in zero magnetization of the ferrofluid. When a magnetic field is applied, alignment of the magnetic dipoles is favored in the same direction as the

(12) Fannin, P. C. *Adv. Chem. Phys.* **1998**, *104*, 181.

(13) de Gennes, P. G.; Pincus, P. A. *Phys. Kondens. Mater.* **1970**, *11*, 189.

(14) Weis, J. J. *Mol. Phys.* **1998**, *93*, 361.

(15) Tavares, J. M.; Weis, J. J.; Telo da Gama, M. M. *Phys. Rev. E* **1999**, *59*, 4388.

(16) Chantrell, R. W.; Bradbury, A.; Popplewell, J.; Charles, S. W. *J. Appl. Phys.* **1982**, *53*, 2742.

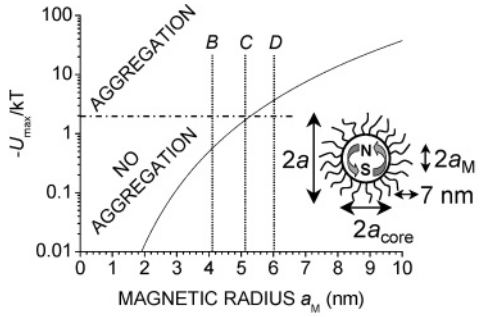

Figure 3. Theoretical calculation of the maximum interaction energy $-U_{max}/k_BT$ between two iron particles with a 7-nm-thick organic surface layer and a magnetic radius a_M 1.5-nm smaller than the iron core radius a_{core}, plotted as a function of a_M (eq 3). For ferrofluids B−D, the experimental magnetic radii are indicated. The inset illustrates the different types of radii used to describe the particles in the text.

magnetic field because the particles are (super)paramagnetic. The interaction energy of a dipole of magnetic moment μ aligned with a magnetic field H equals $\mu_0\mu H$. The average degree of alignment of the magnetic dipoles depends on the ratio of $\mu_0\mu H$ to k_BT because thermal motion tends to destroy the alignment. For noninteracting monodisperse particles, the average magnetization M of the ferrofluid as a function of the external magnetic field is given by the Langevin equation

$$M = M_S[\coth(\mu_0\mu H/k_BT) - (k_BT/\mu_0\mu H)] \quad (4)$$

where M_S is the saturation magnetization and it is assumed that all particles have the same magnetic dipole moment μ. This equation accounts for the general shape of the magnetization curve.

In the low-magnetic-field limit, magnetization is linear with the external magnetic field, and the proportionality factor is called the magnetic susceptibility χ:

$$M = \chi H \quad (5)$$

According to eq 4, the steady-state value χ_0 of the magnetic susceptibility in the low-magnetic-field limit is given by

$$\chi_0 = \mu_0\mu M_S/3k_BT \quad (6)$$

In the high-magnetic-field limit, all magnetic dipoles point in the same direction and the magnetization of the ferrofluid is given by

$$M_S = N\mu \quad (7)$$

where N is the number of particles per unit volume.

The measurement of a magnetization curve allows the determination of the ratio of χ_0 to M_S, from which the magnetic dipole moment μ can be calculated (eq 6). In the case of separate spherical particles, the magnetic radius can then be calculated using eq 1. For an aggregate, the magnetic dipole moment depends on the number of magnetic particles as well as on their spatial positions, orientations, and sizes.

Magnetization in an Alternating Magnetic Field. When the external magnetic field H is changed, a new steady-state magnetization is not reached right away because reorientation of the magnetic dipole moments takes time. In the low-field limit, the rate at which the magnetization M goes toward the steady-state magnetization χ_0H can be assumed to be proportional to the difference between the two:

$$dM/dt = -\omega_{char}(M - \chi_0H) \quad (8)$$

where t is time and ω_{char} is the rate constant in s^{-1}, a characteristic frequency. One way to study the reorientation rate is by applying a weak alternating magnetic field

$$\tilde{H} = H_0 \exp(i\omega t) \quad (9)$$

where H_0 is the amplitude of the magnetic field modulation ("weak" means $\mu_0\mu H_0 \ll k_BT$), $i = \sqrt{(-1)}$, and ω is the radial frequency in s^{-1} (2π times the frequency in Hz). The alternating magnetic field induces a harmonic change in the magnetization, $\tilde{M}$, so that eq 8 can be rewritten as

$$i\omega\tilde{M} = -\omega_{char}(\tilde{M} - \chi_0\tilde{H}) \quad (10)$$

Solving for $\tilde{M}$ leads to

$$\tilde{M} = [\omega_{char}/(\omega_{char} + i\omega)]\chi_0\tilde{H} \quad (11)$$

The dynamic magnetic susceptibility can now be defined as the ratio of $\tilde{M}$ to $\tilde{H}$:

$$\chi(\omega) = \tilde{M}/\tilde{H} = [\omega_{char}/(\omega_{char} + i\omega)]\chi_0 \quad (12)$$

This can be split into a *real* (in-phase) part χ' and an *imaginary* (out-of-phase) part χ'':

$$\chi(\omega) = \chi'(\omega) - i\chi''(\omega) \quad (13)$$

$$\chi'(\omega) = [\omega_{char}^2/(\omega_{char}^2 + \omega^2)]\chi_0 \quad (14a)$$

$$\chi''(\omega) = [\omega\omega_{char}/(\omega_{char}^2 + \omega^2)]\chi_0 \quad (14b)$$

In the low-frequency limit, when $\omega \ll \omega_{char}$, the alternating magnetic susceptibility has a value that corresponds to the initial slope χ_0 of the steady-state magnetization curve. In the high-frequency limit, when $\omega \gg \omega_{char}$, the orientations of the magnetic dipole moments cannot keep up with the alternating magnetic field, and the dynamic magnetic susceptibility is 0. The imaginary component is maximal at $\omega = \omega_{char}$.

When the magnetic dipole moment is free to move within the particles (Néel rotation), the characteristic frequency is given by

$$\omega_N = 2\pi f_0 \exp[-KV/(k_BT)] \quad (15)$$

where f_0 is in the 10^7-10^{12} Hz range[12,17] and is often assumed to be on the order of 10^9 Hz,[2,3] K is a material- and shape-dependent anisotropy constant, and V is the magnetic domain volume, that is, $(4/3)\pi a_M^3$ for a spherical domain.

When the magnetic dipole moment has a fixed orientation within the particles, a change in the orientation of the magnetic dipole moment requires rotation of the entire particle or aggregate. For single spherical particles, the characteristic frequency of Brownian rotational diffusion is given by[12]

$$\omega_B = 2D_r = k_BT/(4\pi\eta a_h^3) \quad (16)$$

where D_r is the rotational diffusion coefficient, η is the

(17) Xiao, G.; Liou, S. H.; Levy, A.; Taylor, S. N.; Chien, C. L. *Phys. Rev. B* **1986**, *34*, 7573.

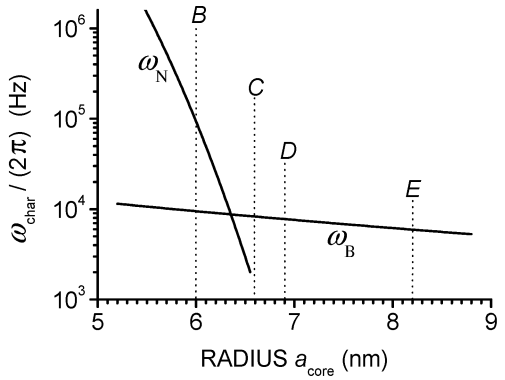

Figure 4. Theoretical calculation of the Néel rotation frequency ω_N (eq 15) and the Brownian rotation frequency ω_B of single particles as a function of the iron core radius a_{core} (eq 16, $\eta = 2.5 \times 10^{-3}$ kg m^{-1} s^{-1}). The particles are assumed to be spherical, with $a_h = a_{core} + 7.0$ nm and $a_{core} = a_M + 1.5$ nm. The calculation of ω_N is based on $f_0 = 10^9$ Hz and $K = 100$ kJ m^{-3}, chosen to reproduce the observed dominance of the Néel or the Brownian mechanism for ferrofluids B−E (see Discussion). The experimental iron core radii from TEM are indicated.

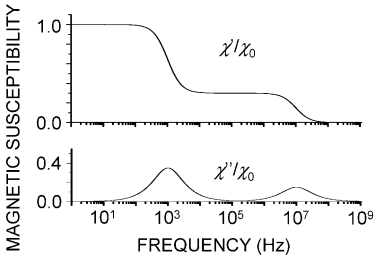

Figure 5. Theoretical calculation of the dynamic magnetic susceptibility as a function of the frequency (real and imaginary components) for a ferrofluid with two populations of particles, with characteristic frequencies of 1 kHz and 10 MHz, respectively (eqs 13 and 14).

viscosity of the solvent, and a_h is the hydrodynamic radius of the particle. The latter can be slightly larger than the physical radius a because of a layer of solvent that moves along with the particle.

Characteristic frequencies for Néel and Brownian rotation of single particles are calculated as a function of the radius in Figure 4. The characteristic frequency of the rotational diffusion of aggregates is a subject of Discussion. In principle, both the Néel and Brownian mechanisms can occur simultaneously for the same particles, so that

$$\omega_{char} = \omega_N + \omega_B \qquad (17)$$

When the two mechanisms occur on different time scales, the fastest determines the characteristic frequency. Because of the strong dependence of ω_N on a_M, the rotation of a chosen particle is likely to be determined by only one of the two mechanisms (Figure 4). In ferrofluids C−E, most of the particles show Brownian rotation, and a smaller part shows Néel rotation at much higher frequencies, beyond our experimental range. If two populations of particles had characteristic frequencies of 1 kHz and 10 MHz, respectively, a spectrum as in Figure 5 would be obtained. At 100 kHz (the upper frequency limit of our experiments), the imaginary component of $\chi(\omega)$ is almost 0, in contrast to the real component, because this is in the low-frequency limit of the 10 MHz particles.

In experimental ferrofluids, a distribution of the size of the particles or aggregates leads to a distribution of the characteristic frequency. Figure 6 shows the effect of a

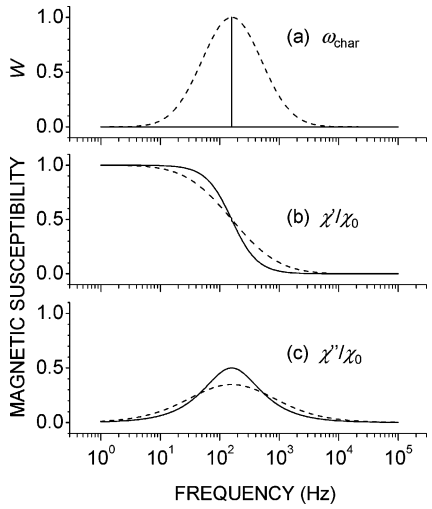

Figure 6. Effect of (a) a log-normal distribution of the characteristic frequency on the frequency dependence of (b) the real and (c) the imaginary components of the dynamic magnetic susceptibility. The curves were calculated using eqs 14 and 18 ($\omega_0 = 1000$ s^{-1}; solid curve, $\sigma = 0$; dotted curve, $\sigma = 0.5$).

Table 1. Iron Core Radii and Concentrations of the Ferrofluids[9−11]

ferrofluid	iron core radius (nm) a_{TEM}	iron core radius (nm) a_{SAXS}	concentration (mass fraction Fe)
B	6.0 ± 0.8	5.3	0.038
C	6.6 ± 1.4	6.0	0.061
D	6.9 ± 1.0	8.8	0.108
E	8.2 ± 1.5	9.5	0.219

log-normal distribution of the characteristic frequency:

$$W = \exp\{-[\log(\omega_{char}) - \log(\omega_0)]^2/[2\sigma^2]\} \qquad (18)$$

where W gives the relative contribution of particles with a characteristic frequency ω_{char} to the susceptibility spectrum, ω_0 is the average characteristic frequency, and σ is the standard deviation. When σ increases, the inflection point of the real component of $\chi(\omega)$ and the maximum of the imaginary component remain at the same frequency. However, the transition from the low- to the high-frequency limit is spread out across a wider frequency range. Moreover, the maximum of the bell-shaped curve of the imaginary component is relatively lower.

Experimental Section

The synthesis and characterization of the iron ferrofluids are also described elsewhere.[9−11] In brief, iron particles coated with modified polyisobutene[18] (2400 g mol^{-1}) were obtained by thermal decomposition of iron carbonyl in a solution of polyisobutene in Decalin, in a similar way as that described by Pathmamanoharan et al.[18] The ferrofluids were characterized using different techniques, including TEM (Figure 1) and small-angle X-ray scattering (SAXS). From these measurements, it was deduced that the organic layer at the surface of the iron particles was 6−7-nm thick and that the radii of the iron cores were as listed in Table 1. Different iron core radii are obtained by TEM (a_{TEM}) and by SAXS (a_{SAXS}, obtained from Guinier fits),[9−11] partly because the two techniques give different types of weighted averages. Mössbauer spectroscopy revealed the presence of carbon in the iron cores according to the stoichiometry of $Fe_{0.75}C_{0.25}$.[19] The saturation magnetization of this material is 1.49×10^6 A

(18) Pathmamanoharan, C.; Zuiverloon, N. L.; Philipse, A. P. *Prog. Colloid Polym. Sci.* **2000**, *115*, 141.

(19) Goosens, A.; de Jongh, L. J.; Butter, K.; Philipse, A. P.; Craje, M. W. J.; van der Kraan, A. M. *Hyperfine Interact.* **2002**, *141*, 381.

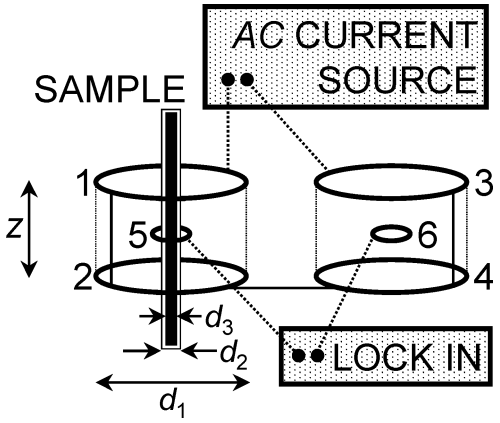

Figure 7. Schematic illustration of the dynamic magnetic susceptibility setup.

m^{-1},[20] slightly lower than that of pure iron[21] (1.71×10^6 A m^{-1}). The concentrations in Table 1 were determined by elemental analysis.

The dynamic magnetic susceptibility was measured at room temperature (20 °C) across the $1-10^5$ Hz range using a home-built setup with mutually inducting coils schematized in Figure 7. An alternating current $\tilde{I}$ with an amplitude of 10 mA was passed through two sets of identical primary coils (coils 1−4) in Helmholtz configuration connected in series (diameter $d_1 = 57.5$ mm, $N_1 = 2 \times 110$ turns per coil, height difference $z = 30$ mm between coils 1 and 2 and between coils 3 and 4). This generated homogeneous alternating magnetic fields and produced alternating voltages in two identical secondary coils (5 and 6, diameter $d_2 = 10.0$ mm, $N_2 = 220$ turns per coil) positioned halfway between the primary coils. A lock-in amplifier measured the amplitude and phase of the difference $\tilde{V}_{56}$ in alternating voltage between the two secondary coils (coils 5 and 6), which is proportional to the susceptibility of the ferrofluid sample placed inside secondary coil 5 (secondary coil 6 was kept empty). The ferrofluid was contained in a hermetically sealed glass tube with an internal diameter d_3 of 5.0 mm. The alternating voltage difference $\tilde{V}_{56}$ was corrected for the weak signal of a glass tube filled with solvent. The magnetic susceptibility of the ferrofluid was calculated using the following equation:

$$\chi = \frac{i\tilde{V}_{56}}{\tilde{I}} \frac{2(d_1^2 + z^2)^{3/2}}{f\mu_0\pi^2 d_1^2 d_3^2 N_1 N_2} \qquad (19)$$

where f is the frequency in Hz.

Magnetic susceptibilities determined in this way were in quantitative agreement with a Kappabridge KLY-3 susceptibility meter (Agico) at its operating frequency of 875 Hz. The reliability of the latter equipment itself was verified by measuring the diamagnetic susceptibility of various solvents, which were in agreement with the literature.[21] The phase of the dynamic susceptibility measured with the home-built setup was verified using a magnetite ferrofluid with a negligible imaginary component of the dynamic magnetic susceptibility in the frequency range of our experiments.

The interaction energy $\mu_0\mu H$ of the alternating magnetic field (30 A m^{-1} amplitude) with the iron particles used was on the order of 10^{-2} k_BT. On this basis, it is assumed that the forces exerted on the particles and aggregates were negligible and did not alter the systems. This assumption is supported by the observation that the spectra measured at 10 or 100 times lower amplitude were the same, except for a lower signal-to-noise ratio. The height of the glass tube containing the ferrofluid could be varied with respect to the coils. Height-resolved susceptibility measurements performed in this way indicated that the ferrofluids were stable at least over a period of several months. The frequency-dependent measurements that are presented were performed at a single height, halfway up the column of ferrofluid, which was 10-cm high.

(20) Bauer-Grosse, E.; Le Caer, G. *Philos. Mag. B* **1987**, *56*, 485.
(21) *CRC Handbook of Chemistry and Physics*; Weast, R. C., Ed.; CRC Press: Boca Raton, 1987.

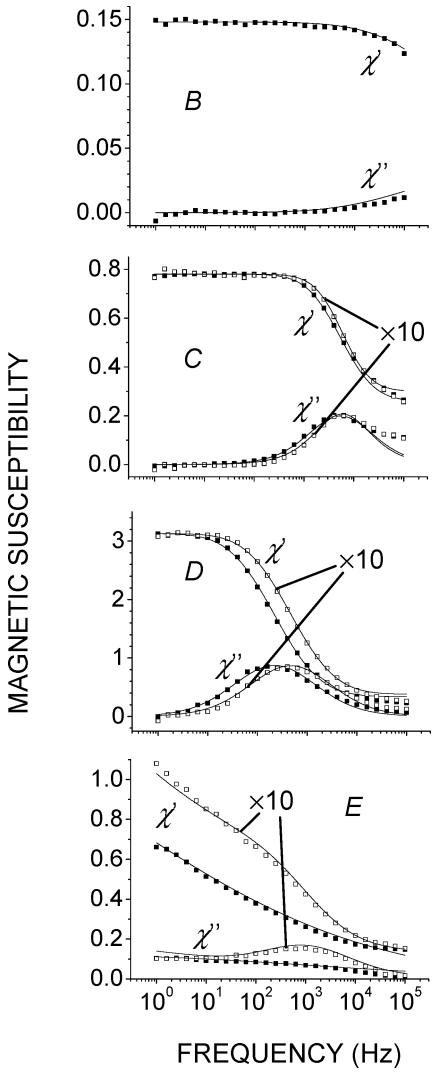

Figure 8. Frequency dependence of the real (χ') and imaginary (χ'') components of the magnetic susceptibility of ferrofluids B−E. Measurements performed after dilution by a factor of 10 have been rescaled by multiplying the data by a factor of 10 ("×10"). The lines are fits of the data (see Table 2).

Magnetization curves were measured at room temperature using a Micromag 2900 alternating gradient magnetometer (Princeton Measurements Corp.). Samples of about 3 μL were contained in air-tight glass cups, filled in a glovebox. This equipment uses a piezoelectric element to measure the motion of the sample due to a weak alternating magnetic field (amplitude, 700 A m^{-1}) superimposed on the much stronger static magnetic field whose value was scanned from -1.2×10^6 A m^{-1} to $+1.2 \times 10^6$ A m^{-1} at a rate of 6×10^4 A m^{-1} s^{-1}. The frequency of the alternating magnetic field was in the 100−1000-Hz range and corresponded to the mechanical resonance frequency, approximately 250 Hz.

Results

Frequency-dependent magnetic susceptibility measurements of iron ferrofluids B−E are presented in Figure 8. For comparison, measurements performed after dilution by a factor of 10 are also shown (except for B, for which the shape of the spectrum remained the same upon dilution but the amplitude decreased by more than the expected factor of 10, presumably because of the oxidation of iron by residual oxygen in the Decalin used for dilution). In ferrofluids B−D, the low-frequency limit is reached

Table 2. Values of Parameters ω_0 and σ Used To Fit the Measurements in Figure 8 According to Eqs 14 and 18[a]

ferrofluid	$\omega_0/2\pi$ (Hz)	σ	ferrofluid	$\omega_0/2\pi$ (Hz)	σ
B	$\sim 3 \times 10^6$	~1.3	D diluted 10×	470	0.6
C	5500	0.4	E	0.05	4.2
C diluted 10×	5900	0.5	E diluted 10×	0.003	3.3
D	220	0.6		1500	0.7

[a] Ferrofluids C−E also contain particles with an average characteristic frequency ($\omega_0/2\pi$) above 10^6 Hz.

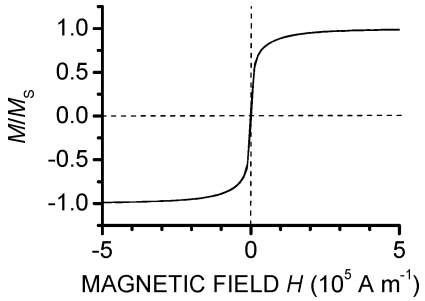

Figure 9. Magnetization M of ferrofluid D (scaled to the saturation magnetization M_S) as a function of the external magnetic field H determined using a weak alternating magnetic probe field at 250 Hz (no hysteresis between forward and backward scans).

(frequency-independent real component, 0 imaginary component), in contrast to ferrofluid E. In none of the systems is the high-frequency limit ($\chi = 0$) reached. The measurements on C−E correspond to the situation simulated in Figure 5, with at least two populations of particles with different average characteristic frequencies, one of which is in excess of 100 kHz.

The measurements have been fitted using a single log-normal distribution of the characteristic frequency (eq 18) and a frequency-independent offset of χ' due to particles with a characteristic frequency well above 100 kHz. For the diluted E ferrofluid, a second log-normal distribution was also used to fit the measurements. The values of the fit parameters are given in Table 2. For ferrofluid B, the characteristic frequency is above 100 kHz, outside the measurement range. For ferrofluid C, the characteristic frequency is 5.5 kHz and remains about the same after dilution, even by a factor of 100 (not shown). For ferrofluid D, the characteristic frequency is 220 Hz before dilution and 470 Hz after dilution. Dilution by a factor of 100 increases the characteristic frequency further (not shown). The measurements on ferrofluid E correspond to a very wide distribution of the characteristic frequency. Before dilution, the data can be fit using a log-normal distribution around an average characteristic frequency lower than 1 Hz, with a standard deviation of a few logarithmic units. After dilution, there are two populations of particles, one similar to the distribution before dilution and another with a characteristic frequency of about 1.5 kHz.

Magnetization curves of ferrofluids B−E were measured to determine the magnetic radius from the initial slope and the saturation magnetization (eqs 1, 6, and 7). As an example, Figure 9 shows the curve for ferrofluid D. No hysteresis was observed between the forward and the backward scans of the magnetic field, except for ferrofluid E. For the latter system, no steady-state magnetization curve could be obtained: the hysteresis loop depended on the magnetic-field-scan history of the sample. This is in line with the slow dynamics of ferrofluid E revealed in Figure 8. For ferrofluids B−D, magnetic radii of 4.1, 5.1, and 6.0 nm were determined, respectively. As expected (see Theory), the magnetic radii are somewhat smaller than the iron core radii from TEM (Table 1). However, for ferrofluid D, the calculated radius does not directly correspond to single particles because aggregates are present (Figure 1) and the frequency of the magnetic probe of the magnetometer (250 Hz) is above the frequency range where the slope of the magnetization curve corresponds to the low-frequency limit of the magnetic susceptibility (which is below about 10 Hz for ferrofluid D, see Figure 8).

Discussion

The results are discussed separately for each member of the series of iron ferrofluids, starting with the system with the smallest magnetic particles.

Ferrofluid B. The characteristic frequency for thermal rotation of the magnetic dipole moment in ferrofluid B is well above 100 kHz (Figure 8 and Table 2). Considering the physical radius of the particles (from TEM), 6-nm iron + 7-nm organic surface layer, this frequency is too high to correspond to the Brownian rotational diffusion of single particles, which would have led to a characteristic frequency of about 10 kHz (Figure 4). It must, therefore, be caused by Néel rotation of the magnetic dipole moment inside the particles.

When the particles are just slightly larger than those in ferrofluid B, Néel rotation of the magnetic dipole moment inside the particles no longer is faster than Brownian rotation of the particles in the solvent. It was already seen in the Theory section that the characteristic frequency for Néel rotation is given by

$$\omega_N = 2\pi f_0 \exp[-KV/(k_B T)] \qquad (15)$$

In Figure 4, the observed threshold above which Brownian rotation becomes the dominant mechanism could be reproduced by assuming that $f_0 = 10^9$ Hz and $K = 100$ kJ m^{-3}. Although that value of f_0 has often also been assumed in the past,[2,3] there are measurements on iron that indicate that a better value for f_0 is 10^{12} Hz,[17] in which case the anisotropy constant K of our particles would be about 175 kJ m^{-3}. From either estimate, the magnetic anisotropy of our particles is 1 order of magnitude larger than the bulk magnetocrystalline anisotropy of iron ($\approx$12 kJ m^{-3}).[22] The reason is probably that, in single domain particles, the magnetocrystalline anisotropy is not the main contribution: other terms such as the surface anisotropy are more important.[17]

Ferrofluid C. For most particles in ferrofluid C, the characteristic frequency for thermal rotation is about 5.5 kHz (Figure 8 and Table 2). Considering the radius of the particles, 6.6-nm iron (from TEM) + 7-nm organic surface layer, this frequency is on the order expected for the Brownian rotational diffusion of single particles (Figure 4). This indicates that the Brownian rotation of the particles is uncorrelated, in agreement with the absence of aggregates seen by cryo-TEM (Figure 1). For the same reason, the characteristic frequency does not change when the ferrofluid is diluted, and the slope of the magnetization curve corresponds to the magnetic moment of single particles ($\mu = 8.4 \times 10^{-19}$ A m^2).

When eq 16 is used, the log-normal characteristic frequency distribution can be converted into a hydrodynamic radius distribution, leading to Figure 10. The hydrodynamic radius of 16 ± 6 nm is slightly larger than the physical radius of about 14 nm (iron core radius a_{TEM} = 6.6 ± 1.4 nm, organic layer thickness 6−7 nm). In

(22) Jiles, D. *Introduction to Magnetism and Magnetic Materials*; Chapman & Hall: London, 1991.

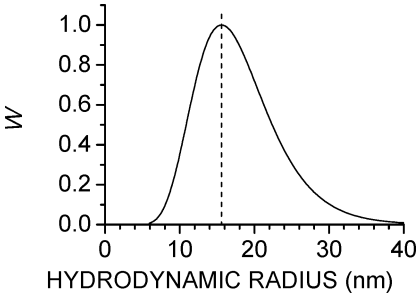

Figure 10. Hydrodynamic radius (a_h) distribution calculated from the characteristic frequency distribution of ferrofluid C (Table 2) using eq 16 ($\eta = 2.5 \times 10^{-3}$ kg m^{-1} s^{-1}). The vertical dotted line indicates the average radius.

principle, the hydrodynamic radius can include a solvent layer and is affected by particle roughness and nonsphericity. The larger standard deviation than that of the iron core radius can be due to a distribution of the surface layer thickness and of the particle shape.

Part of the particles in ferrofluid C appears to have a characteristic frequency above 100 kHz, indicating Néel rotation as in ferrofluid B. These are the smallest C particles, although they do not have to be much smaller than the average C particle because the transition from Néel to Brownian rotation as function of the particle size is quite abrupt (Figure 4).

Ferrofluid D. In ferrofluid D, a minor part of the magnetic dipoles has a thermal rotation frequency above 100 kHz and the major part has a broad distribution of the characteristic frequency around 220 Hz. Néel rotation occurs for the particles with a characteristic frequency above 100 kHz. However, the 220-Hz characteristic frequency of most particles is well below that for the Brownian rotation of single particles (about 5.9 kHz, Figure 4) and must correspond to the rotational diffusion of aggregates. These observations agree with cryo-TEM, which shows a population of single particles and a population of particles present in aggregates of a few particles.

In principle, there is insufficient information to deduce the number N of particles per aggregate from the characteristic rotation frequency. The Brownian rotation rate should depend on the size, shape, and rigidity of the individual particles and of the aggregates that they form. Nevertheless, a rough estimate will now be made of how the characteristic frequency depends on N to illustrate how much the rotational diffusion can slow even when relatively small aggregates are formed. The estimate is based on the formula of Tiroda et al.[23−25] for the rotational diffusion coefficient of spherocylinders with an aspect ratio $L/d \geq 2$, where L is the rod length and d is the cross-sectional diameter. By dividing that expression by eq 16 for the Brownian rotation of a single spherical particle and by interpreting the length-to-thickness ratio of the spherocylinder as a measure for N, the following relation is obtained ($N \geq 2$):

$$\omega_{chain}/\omega_{single} \approx (3/N^3)(\ln N - 0.662 + 0.917N^{-1} - 0.050N^{-2}) \quad (20)$$

where ω_{chain} is the characteristic frequency for the rotational diffusion of a chain of N particles and ω_{single} is the characteristic frequency for a single particle. The ratio $\omega_{chain}/\omega_{single}$ calculated using eq 20 is plotted as a function of N in Figure 11. It can be seen that the formation of aggregates of four particles is sufficient to decrease the rotational diffusion rate by a factor of 25 compared to the rotational diffusion rate of single particles. The factor of 25 corresponds to the ratio $\omega_{chain}/\omega_{single}$ for ferrofluid D (before dilution), whose aggregates indeed contain about four particles. According to cryo-TEM, the average number of particles per aggregate is 3.6 if single particles are left out of the average.

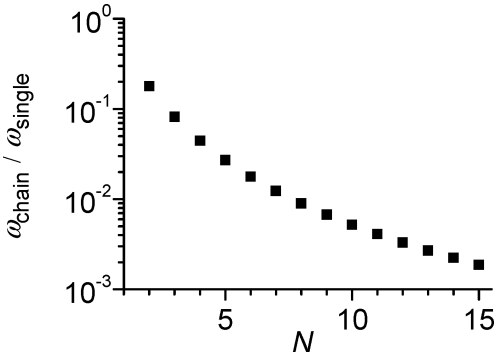

Figure 11. Ratio of the rotational diffusion frequency ω_{chain} of a chain of N particles to the rotational diffusion frequency ω_{single} of a single particle according to eq 20.

Upon dilution, the characteristic frequency goes up, which indicates that the size of the aggregates goes down (Figure 8 and Table 2). This suggests that the size of the aggregates is determined by a dynamic equilibrium. If single magnetic particles can reversibly join an aggregate or leave it, the size of the aggregates results from the competition between both processes, and it is possible to have a small steady-state number of particles per aggregate. The lower the concentration of single particles, the more the dynamic equilibrium shifts toward small aggregates. If aggregation were irreversible, aggregates would only be able to grow in size and would not shrink upon dilution.

According to eq 3, the maximum magnetic attraction energy of two particles in ferrofluid D is on the order of $3k_BT$, assuming a rigid organic surface layer of 7 nm and a difference of 1.5 nm between a_{core} (from TEM) and a_M. This agrees with results by other authors, who found aggregation starting at an attraction energy of $2-2.5k_BT$.[13−16] In an aggregate, the distance between two particles is likely to be somewhat closer because of the flexibility of the organic surface layer, leading to an even higher attraction energy. In ferrofluid C, the maximum attraction between two particles is about $1.6k_BT$ (Figure 3), which apparently is insufficient for the formation of aggregates.

Ferrofluid E. As in ferrofluid D, a minor part of the particles in ferrofluid E exhibits Néel rotation of the magnetic moment, and the major part of the particles is in aggregates. Judging from the much lower characteristic frequencies in ferrofluid E (Figure 8 and Table 2), the aggregates are much larger than those in ferrofluid D. This is in agreement with cryo-TEM (Figure 1).

Upon dilution, a second population of particles appears with a characteristic frequency of about 1.5 kHz. This frequency is too low to correspond to the rotation of single particles. According to eq 20, it is probably due to aggregates of two particles. If the size of the aggregates results from a dynamic equilibrium and the particles were monodisperse, a smooth distribution of the aggregate size

(23) Tirado, M. M.; Garcia de la Torre, J. *J. Chem. Phys.* **1979**, *71*, 2581.
(24) Tirado, M. M.; Garcia de la Torre, J. *J. Chem. Phys.* **1980**, *73*, 1986.
(25) Garcia de la Torre, J.; López Martinez, M. C.; Tirado, M. M. *Biopolymers* **1984**, *23*, 611.

would be expected instead of two separate populations. However, the particles are not monodisperse, which means that strong differences occur in the interaction energy between neighboring particles (see Figure 3). This can vary from a few $k_B T$, as in ferrofluid D, to energies that are several times larger. It is likely that the smaller particles in ferrofluid E can reversibly adsorb and desorb, whereas the larger particles remain almost irreversibly stuck to each other.

Conclusions

The dynamic susceptibility spectrum of a ferrofluid is sensitive to the presence of aggregates. The ferrofluids for which aggregates were observed by cryo-TEM, ferrofluids D and E (Figure 1), have much slower rotational diffusion rates than those expected for single particles (Figure 8). The number of particles in the aggregates is difficult to estimate on the basis of the rotational diffusion rate, because it also depends on the shape and flexibility of the aggregates. Nevertheless, the increase in the rotational diffusion rate upon dilution indicates that the size of the aggregates decreases. This suggests that the size of the aggregates results from a dynamic equilibrium between the sticking of particles to each other and unsticking, with a distribution in the interaction strength between neighboring particles due to polydispersity.

The ferrofluids without any aggregates, according to cryo-TEM, ferrofluids B and C, have much higher rotational diffusion rates. From the rotational diffusion rate of the C particles, the hydrodynamic radius of the particles could be calculated. In ferrofluid B, the magnetic moment rotated inside the particles so that no information could be obtained about the rotational diffusion of the particles. The threshold size above which Brownian rotation is faster than Néel rotation suggests that Néel rotation is relatively slow in our particles, probably because of surface anisotropy.

The presence and size of aggregates is very sensitive to particle size. The parallels between the cryo-TEM and the dynamic susceptibility measurements indicate that when aggregates occur in the two-dimensional geometry of cryo-TEM, they also occur in the three-dimensional geometry of the susceptibility measurements. The apparent explanation is that the interaction energy required for aggregation is practically the same in two and in three dimensions. The combination of cryo-TEM with dynamic magnetic susceptibility measurements appears to be a powerful approach to study aggregation in model (monodisperse) magnetic fluids. Cryo-TEM gives direct images of aggregates, although only in two dimensions and without a good control of the concentration. Frequency-resolved magnetic susceptibility measurements are at least in qualitative agreement with cryo-TEM, and they make it possible to study three-dimensional aggregation as a function of the concentration.

Acknowledgment. We thank Prof. Dr. A. P. Philipse for helpful discussions and for initiating our work on iron ferrofluids. We also thank Dr. M. Raşa for helpful discussions, Drs. T. Arts for work on the software and for performing preliminary measurements, and Mr. C. Rietveld for helping to construct the experimental setup.

LA0346393